International Journal of Multidisciplinary Research and Growth Evaluation.

Earth engine application to retrieve long-term terrestrial and aquatic time series of satellite reflectance data

Ritika Prasai
Department of Biology, Baylor University, Waco, Texas, USA

* Corresponding Author: **Ritika Prasai**

Article Info

ISSN (online): 2582-7138
Volume: 03
Issue: 03
May-June 2022
Received: 09-04-2022
Accepted: 24-04-2022
Page No: 165-171
DOI: https://doi.org/10.54660/anfo.2022.3.3.11

Abstract

Google earth engine is an open source cloud based computing platform that is designed to process large scale datasets. Owing to its capacity and features, it can be useful to wide range of applications-the most prominent being vegetation mapping and monitoring, earth sciences related studies and many others. We have developed a web tool based on google earth engine to encourage and assist the researchers from non-programming background to use google earth engine. This application is freely available and can be accessed at https://mapcoordinates.info/. In the current version, this application has some interesting features like data filter, generates time series plots, time series records and metadata in .csv format. Users can download the time series records of any location, select the satellite sensor, choose the model, filter the cloud cover, scale factor. This application also visualizes the time slider feature for the location selected on the map.

Keywords: Google earth engine, database, open source, Python, web-based application, timeseries

1. Introduction

Google earth engine is an open source cloud based computing platform that is designed to process large scale datasets (Prasai *et al*., 2021, Inman & Lyons, 2020, Gorelick *et al*., 2017, Midekisa *et al*., 2017) [31, 8, 6, 17]. Users do not require the latest computers or software to work on big data (Phan *et al*., 2020, Thieme *et al*., 2020) [27, 34]. Owing to its capacity and features, it can be useful to wide range of applications-the most prominent being vegetation mapping and monitoring (Venkatappa *et al*., 2019, Wang *et al*., 2015) [35, 36], disaster management (Xia *et al*., 2019) [38], earth sciences related studies and many others (Prasai *et al*., 2021) [31]. We have developed a web tool based on google earth engine to encourage and assist the researchers from non-programming background to use google earth engine. This application is freely accessible and available at https://mapcoordinates.info/. This tool extracts the datasets from the google earth engine database. It uses Python API to interact with google earth engine database. In the current version, this application has some interesting features like data filter, generates time series plots, time series records and metadata in .csv format. Users can download the time series records of any location, select the satellite sensor, choose the algorithm to process the datasets, filter the cloud cover, scale factor. This application also visualizes the time slider feature for the location selected on the map.

2. Data and Methods

2.1. Conceptual Framework

https://mapcoordinates.info/ has a web-client as the front-end and GEE as computing back-ends. The front end is the graphical user interface (GUI) web client where the users can specify the algorithms, date range, filter the datasets and send requests to run the analyses (Figure 1). We used Ipywidgets a python based library, HTML and CSS to design GUI/front end of this application. Since all storages and computing operations are made on the cloud (GEE), the web-client can be accessed from any browser supporting device such as mobile, laptop or desktop computing devices.

However, the framework is developed mainly with PC environments in mind and thus it is not optimized for mobile applications. The back end uses GEE to access satellite data, conduct the analyses and use Google's cloud computing capabilities. We used Python API to interact with GEE backend. Current version of this tool has 3 algorithms (NDVI/NDCI), 2 BDA, Turbidity Index). We can select the location using polygon icon present on the left corner of the tool. It provides time slider to detect the changes on the map. Users can filter the datasets based on scale, clouds cover, dates. They get the time series datasets and metadata in .csv format and plots after passing request through submit button present on the GUI.

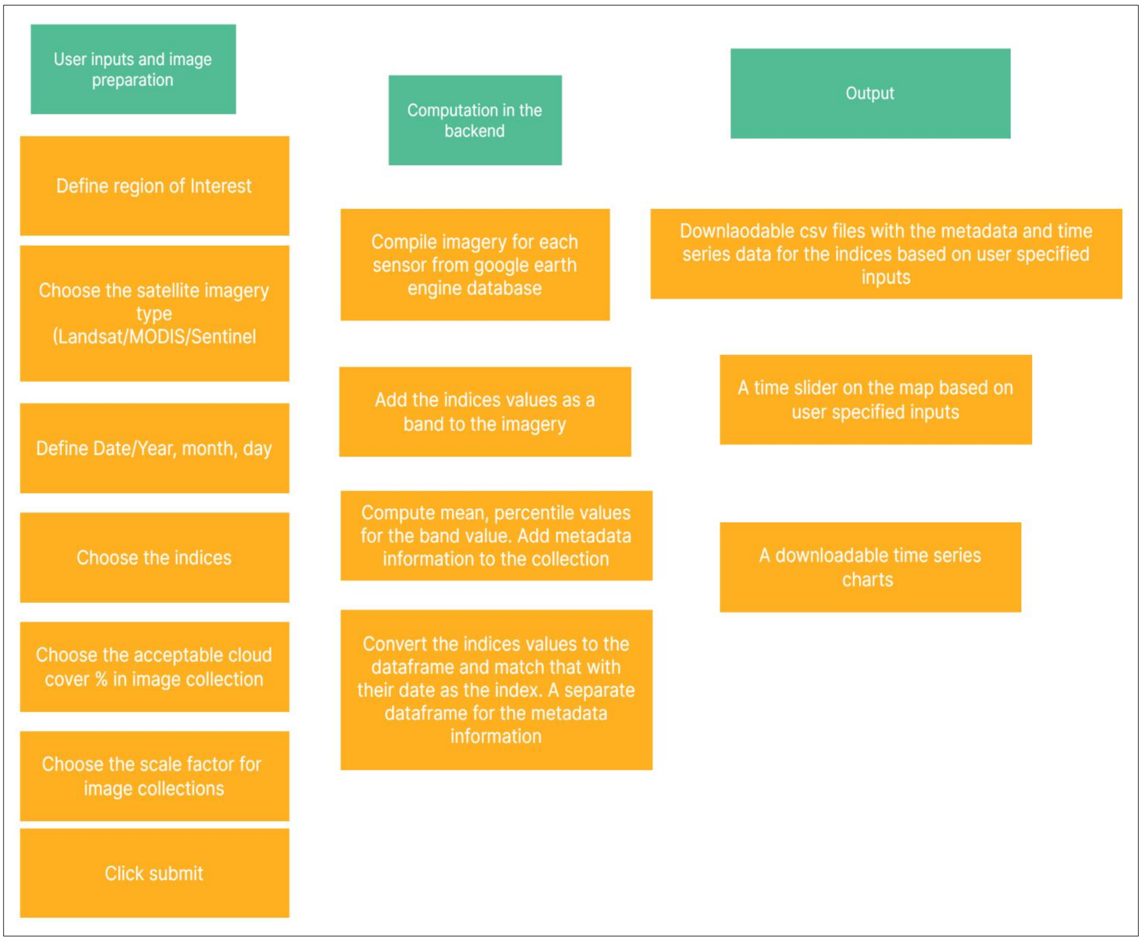
User inputs and image preparation
Define region of Interest
Choose the satellite imagery type (Landsat/MODIS/Sentinel
Define Date/Year, month, day
Choose the indices
Choose the acceptable cloud cover % in image collection
Choose the scale factor for image collections
Click submit
Computation in the backend
Compile imagery for each sensor from google earth engine database
Add the indices values as a band to the imagery
Compute mean, percentile values for the band value. Add metadata information to the collection
Convert the indices values to the dataframe and match that with their date as the index. A separate dataframe for the metadata information
Output
Downlaodable csv files with the metadata and time series data for the indices based on user specified inputs
A time slider on the map based on user specified inputs
A downloadable time series charts

Fig 1: Flow chart describing the overall application design

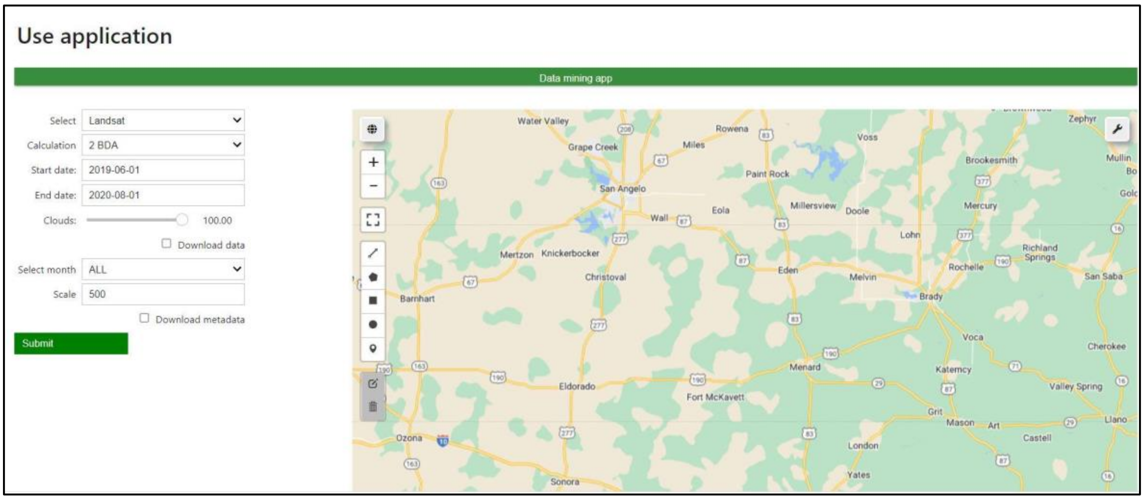
Use application

Data mining app

Select: Landsat

Calculation: 2 BDA

Start date: 2019-06-01

End date: 2020-08-01

Clouds: 100.00

□ Download data

Select month: ALL

Scale: 500

□ Download metadata

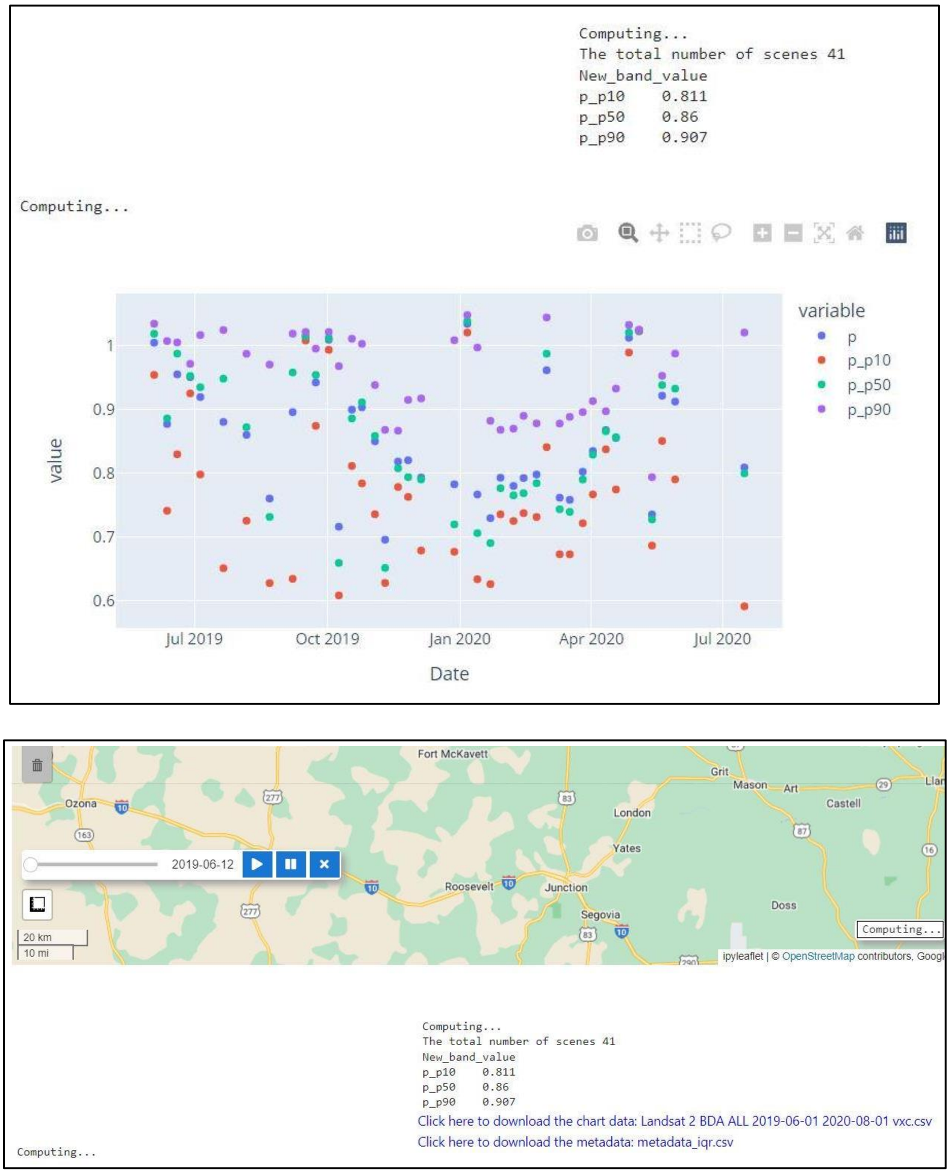

```
Computing...
The total number of scenes 41
New_band_value
p_p10    0.811
p_p50    0.86
p_p90    0.907
```

```
Computing...
```

```
Computing...
The total number of scenes 41
New_band_value
p_p10    0.811
p_p50    0.86
p_p90    0.907
```

Click here to download the chart data: Landsat 2 BDA ALL 2019-06-01 2020-08-01 vxc.csv

Click here to download the metadata: metadata_iqr.csv

```
Computing...
```

Source: Video link: https://www.youtube.com/watch?v=jgkYn6oyucY

Fig 2: GUI of the application

2.2. Data

We have included three satellite imagery in the current version: Landsat (1984-current), Sentinel (2015-current) and MODIS (2000-current). We used these datasets from the google earth engine database.

2.2.1. Landsat Datasets

We used Landsat collection 2 tier 1 products available in google earth engine database. These collections include the improved dataset collections over collection 1 which supports recent developments in data processing and algorithm development (Gorelick *et al.*, 2017) [6]. These collections have been corrected using the Landsat Ecosystem Disturbance Adaptive Processing System and Land Surface Reflectance Code software. USGS resampled these collections to a spatial resolution of 30 m using cubic convolution. These collections have been then filtered and images of higher quality have been stored in Tier1.

2.2.1.1. Landsat 8 products

We have included atmospherically corrected surface reflectance datasets from the collection 2 tier 1 collections. These products are derived/produced by the Landsat 8 OLI/TIRS sensors (Gorelick *et al.*, 2017) [6]. These collections include 5 visible and near infrared bands and 2 short wave bands. We have not included thermal band in this collection. These collections are created with the Land Surface Reflectance code (LaSRC) (Gorelick *et al.*, 2017) [6]. More information about this product can be found at (https://developers.google.com/earthengine/datasets/catalog/LANDSAT_LE08_C02_T1_L2.

2.2.1.2. Landsat 7 products

We included atmospherically corrected surface reflectance datasets from the collection 2 tier 1 collections. These datasets contain 4 visible and near-infrared bands and 2 short wave infrared bands which are orthorectified to get surface reflectance, one thermal infrared (TIR) band which is processed to orthorectified surface temperature (Gorelick *et al.*, 2017) [6]. There is also intermediate bands used in the calculation of the ST products as well as QA bands. These products are created with the Landsat Ecosystem Disturbance Adaptive Processing Systems (LEDAPS) algorithm (version 3.4.0) (Gorelick *et al.*, 2017) [6]. More information about the datasets can be found at (https://developers.google.com/earthengine/datasets/catalog/LANDSAT_LE07_C02_T1_L2)

2.2.1.3. Landsat 5 products

We have included surface reflectance and land surface temperature datasets that are atmospherically corrected and derived from the Landsat TM sensor. These datasets contains 4 visible and near-infrared (VNIR) bands and 2 short-wave infrared (SWIR) bands which are processed to obtain orthorectified surface reflectance, and one thermal infrared (TIR) band processed to orthorectified surface temperature (Gorelick *et al*., 2017) [6]. They also contain intermediate bands used in calculation of the ST products, as well as QA bands (Gorelick *et al*., 2017) [6]. These datasets are created with the Landsat Ecosystem Disturbance Adaptive Processing System (LEDAPS) algorithm (version 3.4.0). More information about these datasets can be obtained from the link: https://developers.google.com/earth-engine/datasets/catalog/LANDSAT_LT05_C02_T1_L2

2.2.1.4. Merging Landsat Products

We used merge algorithm to merge the Landsat products. We matched the bands in Landsat 8 with Landsat 7 and Landsat 5 before merging the datasets. We did not include the thermal band from Landsat 8 products while merging the datasets.

2.2.2. MODIS datasets

We have included the datasets that provides an estimate of the surface reflectance of Terra MODIS bands. They have 7 bands and 500m resolution. The datasets is atmospherically corrected for gasses, aerosols and Rayleigh scattering (Gorelick *et al*., 2017) [6]. There are also quality layer and 4 observation bands included (Gorelick *et al*., 2017) [6]. The value for each pixel is selected from all the acquisitions within the 8-day composite on the basis of high observation coverage, low view angle, the absence of clouds or cloud shadow and aerosol loading. More information of the datasets can be found from the link:
https://developers.google.com/earthengine/datasets/catalog/MODIS_006_MOD09A1

2.2.3. Sentinel dataset

This dataset consist high resolution, multi-spectral imaging mission supporting Copernicus Land monitoring. This dataset contains 12 UINT 16 spectral bands representing SR. They were downloaded from scihub and computed by running sen2cor. We used cloud filter to filter out the clouds from the datasets (Gorelick *et al*., 2017) [6]. These datasets are ready to use for monitoring vegetation, soil, water cover as well as observation of inland waterways and coastal areas. More information about the datasets can be found at:
https://developers.google.com/earthengine/datasets/catalog/COPERNICUS_S2_SR#description

2.3. Tools and techniques

We used both existing as well as newly developed scripts to retrieve data, compute and visualize. For example, time slider, plots display on the map are existing source codes we used and we developed source codes to design GUI, algorithms and time series computation and download functionality using GEE Python API. Table 1 shows our method of algorithms development based on dataset/satellite imagery type.

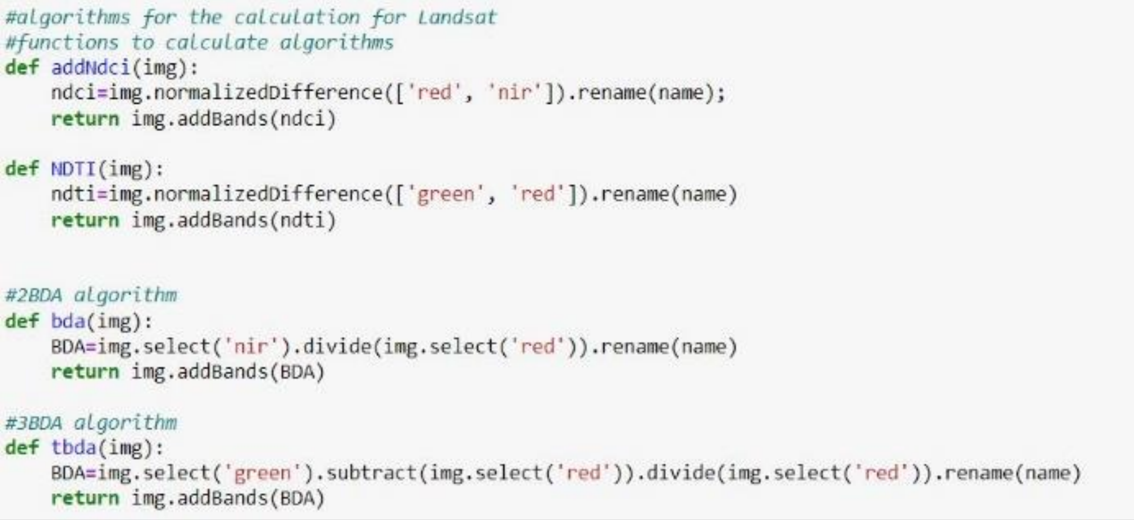

```
#algorithms for the calculation for Landsat
#functions to calculate algorithms
def addNdci(img):
    ndci=img.normalizedDifference(['red', 'nir']).rename(name);
    return img.addBands(ndci)

def NDTI(img):
    ndti=img.normalizedDifference(['green', 'red']).rename(name)
    return img.addBands(ndti)


#2BDA algorithm
def bda(img):
    BDA=img.select('nir').divide(img.select('red')).rename(name)
    return img.addBands(BDA)

#3BDA algorithm
def tbda(img):
    BDA=img.select('green').subtract(img.select('red')).divide(img.select('red')).rename(name)
    return img.addBands(BDA)
```

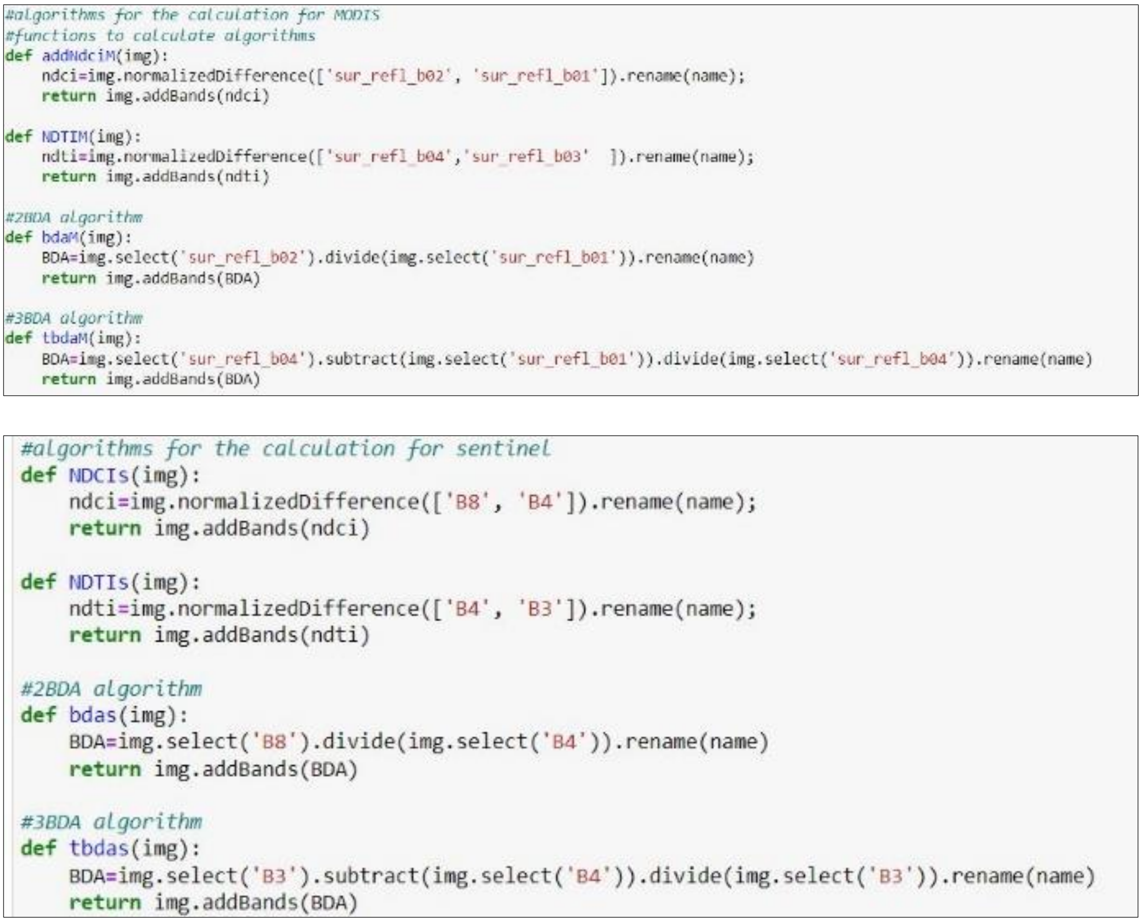

```
#algorithms for the calculation for MODIS
#functions to calculate algorithms
def addNdciM(img):
    ndci=img.normalizedDifference(['sur_refl_b02', 'sur_refl_b01']).rename(name);
    return img.addBands(ndci)

def NDTIM(img):
    ndti=img.normalizedDifference(['sur_refl_b04','sur_refl_b03'  ]).rename(name);
    return img.addBands(ndti)

#2BDA algorithm
def bdaM(img):
    BDA=img.select('sur_refl_b02').divide(img.select('sur_refl_b01')).rename(name)
    return img.addBands(BDA)

#3BDA algorithm
def tbdaM(img):
    BDA=img.select('sur_refl_b04').subtract(img.select('sur_refl_b01')).divide(img.select('sur_refl_b04')).rename(name)
    return img.addBands(BDA)
```

```
#algorithms for the calculation for sentinel
def NDCIs(img):
    ndci=img.normalizedDifference(['B8', 'B4']).rename(name);
    return img.addBands(ndci)

def NDTIs(img):
    ndti=img.normalizedDifference(['B4', 'B3']).rename(name);
    return img.addBands(ndti)

#2BDA algorithm
def bdas(img):
    BDA=img.select('B8').divide(img.select('B4')).rename(name)
    return img.addBands(BDA)

#3BDA algorithm
def tbdas(img):
    BDA=img.select('B3').subtract(img.select('B4')).divide(img.select('B3')).rename(name)
    return img.addBands(BDA)
```

Fig 3: Sample codes used to develop algorithms from the satellite reflectance data

Table 1: Algorithms used in the web-based tool

Sensor Image	Index	Band combination
Landsat	NDVI/NDCI	(Near Infrared-Red)/(Near Infrared + Red)
	2BDA	Near Infrared/Red
	3 BDA	(Green-Red)/(Green + Red)
	TI	(Green-Red)/Red
MODIS	NDVI/NDCI	(Sur_refl_b02- Sur_refl_b01)/ (Sur_refl_b02 + Sur_refl_b01)
	2 BDA	Sur_refl_b02/Sur_refl_b0
	3 BDA	(Sur_refl_b04- Sur_refl_b03)/ (Sur_refl_b04
	TI	(Sur_refl_b04- Sur_refl_b03)/ (Sur_refl_b04 + Sur_refl_b03)
Sentinel	NDVI/NDCI	(B8-B4)/(B8 + B4)
	2 BDA	B8/B4
	3 BDA	(B3-B4)/(B3)
	TI	(B4-B3)/(B4 + B3)

2.3.1. Algorithms used

We used normalized difference vegetation index (NDVI), 2BDA, 3 BDA and Turbidity Index (TI) algorithms in our web-based tool. NDVI is the ratio of red and near infrared bands and used in wide range of research related to assess vegetation health (Gandhi *et al*., 2015; Prasai, 2021) [5, 31]. NDVI is widely used in studying land use land cover (Somayajula *et al*., 2021) [33], habit suitability (Prasai *et al*., 2021) [31], species conservation (Nieto *et al*., 2015) [24], floods and risk mapping (Gabban *et al*., 2006) [4] related research projects. Normalized difference chlorophyll index (NDCI) is also the ratio of red and near infrared bands and used to quantify the chlorophyll pigments in inland water bodies (S. Mishra & Mishra, 2012) [18] 2BDA and 3BDA algorithms are also used to extract chlorophyll concentration in inland water bodies (Buma & Lee, 2020) [3]. TI is one of the water quality parameters and gives information about the clarity of the water (Zheng & DiGiacomo, 2020) [40].

References

1. Augusto-Silva P, Ogashawara I, Barbosa C, de Carvalho L, Jorge D, Fornari C, *et al*. Analysis of MERIS reflectance algorithms for estimating chlorophyll-a concentration in a Brazilian reservoir. Remote Sensing. 2014;6(12):11689-11707. https://doi.org/10.3390/rs61211689.
2. Bai Y, Yang Y, Jiang H. Intercomparison of AVHRR GIMMS3g, Terra MODIS, and SPOT-VGT NDVI products over the Mongolian Plateau. Remote Sensing. 2019;11(17):2030. https://doi.org/10.3390/rs11172030.
3. Buma WG, Lee SI. Evaluation of Sentinel-2 and Landsat 8 images for estimating chlorophyll-a concentrations in Lake Chad, Africa. Remote Sensing. 2020;12(15):2437. https://doi.org/10.3390/rs12152437.
4. Gabban A, San-Miguel-Ayanz J, Viegas DX. On the suitability of the use of normalized difference vegetation index for forest fire risk assessment. International Journal of Remote Sensing. 2006;27(22):5095-5102. https://doi.org/10.1080/01431160500185656.
5. Gandhi GM, Parthiban S, Thummalu N, Christy A. NDVI: Vegetation change detection using remote sensing and GIS-a case study of Vellore District. Procedia Computer Science. 2015;57:1199-1210. https://doi.org/10.1016/j.procs.2015.07.415.

6. Gorelick N, Hancher M, Dixon M, Ilyushchenko S, Thau D, Moore R. Google Earth Engine: Planetary-scale geospatial analysis for everyone. Remote Sensing of Environment. 2017;202:18-27. https://doi.org/10.1016/j.rse.2017.06.031.
7. Hamunyela E, Rosca S, Mirt A, Engle E, Herold M, Gieseke F, Verbesselt J. Implementation of BFAST Monitor algorithm on Google Earth Engine to support large-area and sub-annual change monitoring using earth observation data. Remote Sensing. 2020;12(18):2953. https://doi.org/10.3390/rs12182953.
8. Inman VL, Lyons MB. Automated inundation mapping over large areas using Landsat data and Google Earth Engine. Remote Sensing. 2020;12(8):1348. https://doi.org/10.3390/RS12081348.
9. Johansen R, Beck R, Nowosad J, Nietch C, Xu M, Shu S, Yang B, *et al*. Evaluating the portability of satellite-derived chlorophyll-a algorithms for temperate inland lakes using airborne hyperspectral imagery and dense surface observations. Harmful Algae. 2018;76:35-46. https://doi.org/10.1016/j.hal.2018.05.001.
10. Kim Y, Park NW, Lee KDo. Self-learning based land-cover classification using sequential class patterns from past land-cover maps. Remote Sensing. 2017;9(9):921. https://doi.org/10.3390/rs9090921.
11. Krakauer N, Lakhankar T, Anadón J. Mapping and attributing normalized difference vegetation index trends for Nepal. Remote Sensing. 2017;9(10):986. https://doi.org/10.3390/rs9100986.
12. Le C, Hu C, Cannizzaro J, English D, Muller-Karger F, Lee Z. Evaluation of chlorophyll-a remote sensing algorithms for an optically complex estuary. Remote Sensing of Environment. 2013;129:75-89. https://doi.org/10.1016/j.rse.2012.11.001.
13. Liu X, Zhu X, Li S, Liu Y, Pan Y. Changes in growing season vegetation and their associated driving forces in China during 2001-2012. Remote Sensing. 2015;7(11):15517-15535. https://doi.org/10.3390/rs71115517.
14. Liu Y, Li Y, Li S, Motesharrei S. Spatial and temporal patterns of global NDVI trends: Correlations with climate and human factors. Remote Sensing. 2015;7(10):13233-13250. https://doi.org/10.3390/rs71013233.
15. Luan J, Liu D, Zhang L, Huang Q, Feng J, Lin M, *et al*. Analysis of the spatial-temporal change of the vegetation index in the upper reach of Han River Basin in 2000–2016. Proceedings of the International Association of Hydrological Sciences. 2018;379:287-292. https://doi.org/10.5194/piahs-379-287-2018.
16. Kaymaz ŞM, Ates E. Estimating chlorophyll-a concentration using remote sensing techniques. Annals of Reviews and Research. 2018;4(2):555633.
17. Midekisa A, Holl F, Savory DJ, Andrade-Pacheco R, Gething PW, Bennett A, Sturrock HJ. Mapping land cover change over continental Africa using Landsat and Google Earth Engine cloud computing. PloS one. 2017;12(9):e0184926. https://doi.org/10.1371/journal.pone.0184926.
18. Mishra S, Mishra DR. Normalized difference chlorophyll index: A novel model for remote estimation of chlorophyll-a concentration in turbid productive waters. Remote Sensing of Environment. 2012;117:394-406. https://doi.org/10.1016/j.rse.2011.10.016.
19. Mlenga DH, Jordaan AJ. Integrated drought monitoring framework for Eswatini applying standardized precipitation index and normalized difference vegetation index. Jàmbá Journal of Disaster Risk Studies. 2020;12(1). https://doi.org/10.4102/jamba.v12i1.749.
20. Moses WJ, Gitelson AA, Berdnikov S, Saprygin V, Povazhnyi V. Operational MERIS-based NIR-red algorithms for estimating chlorophyll-a concentrations in coastal waters-the Azov Sea case study. Remote Sensing of Environment. 2012;121:118-124. https://doi.org/10.1016/j.rse.2012.01.024.
21. Moura YM, Galvão LS, dos Santos JR, Roberts DA, Breunig FM. Use of MISR/Terra data to study intra- and inter-annual EVI variations in the dry season of tropical forest. Remote Sensing of Environment. 2012;127:260-270. https://doi.org/10.1016/j.rse.2012.09.013.
22. Mutanga O, Kumar L. Google Earth Engine applications. Remote Sensing. 2019;11(5):591. https://doi.org/10.3390/rs11050591.
23. Nieto S, Flombaum P, Garbulsky MF. Can temporal and spatial NDVI predict regional bird-species richness? Global Ecology and Conservation. 2015;3:729-735. https://doi.org/10.1016/j.gecco.2015.03.005.
24. Novillo CJ, Arrogante-Funes P, Romero-Calcerrada R. Recent NDVI trends in mainland Spain: Land-cover and phytoclimatic-type implications. ISPRS International Journal of Geo-Information. 2019;8(1):43. https://doi.org/10.3390/ijgi8010043.
25. Pedreros-Guarda M, Abarca-del-Río R, Escalona K, García I, Parra S. A Google Earth Engine application to retrieve long-term surface temperature for small lakes. Case: San Pedro Lagoons, Chile. Remote Sensing. 2021;13(22):4544. https://doi.org/10.3390/rs13224544.
26. Phan TN, Kuch V, Lehnert LW. Land cover classification using Google Earth Engine and Random Forest classifier-the role of image composition. Remote Sensing. 2020;12(15):2411. https://doi.org/10.3390/rs12152411.
27. Poddar S, Chacko N, Swain D. Estimation of chlorophyll-a in northern coastal Bay of Bengal using Landsat-8 OLI and Sentinel-2 MSI sensors. Frontiers in Marine Science. 2019;6:598. https://doi.org/10.3389/fmars.2019.00598.
28. Prasai R. Distribution of Bengal Tiger (*Panthera tigris*) and their main prey species in Chitwan National Park, Nepal (Doctoral dissertation, Tarleton State University); c2021.
29. Prasai R, Kafley H, Upadhaya BP, Kandel RC, Lamichhane BR. Comparison of change detection techniques to monitor spatial and temporal dynamics of forest cover in Chitwan National Park, Nepal. The Indian Forester. 2016;142(12):1231-1238.
30. Resende AF, Nelson BW, Stark SC, Richardson AD, Galvão LS, Wu J, *et al*. Turning the point: Improving leaf area index estimates with airborne lidar by quantifying leaf clumping and woody contributions. Remote Sensing of Environment. 2020;240:111678. https://doi.org/10.1016/j.rse.2020.111678.
31. Resende AF, Stark SC, Valbuena R, Solórzano LA, Overbeck GE, Guimarães JF, *et al*. Quantifying and modelling the structure and biomass of the Brazilian savanna vegetation using earth observation and field data. Plant Ecology & Diversity. 2021;14(2):113-130. https://doi.org/10.1080/17550874.2021.1886527.

32. Singh A, Singh PM, Kumar L. Remote sensing of chlorophyll-a: Review of methods and applications. Journal of the Indian Society of Remote Sensing. 2020;48(3):407-426. https://doi.org/10.1007/s12524-019-01083-w.
33. Sinha P, Kumar L, Reid N. Remote sensing of successional changes in regrowth forest in sub-tropical Australia using MODIS and Landsat time-series. Remote Sensing. 2015;7(11):14002-14029. https://doi.org/10.3390/rs71114002.
34. Soulard CE, Sleeter BM, Auch RF, Drummond MA, Sayler KL, Wilson TS. Land use and land cover in the conterminous United States from 1974 to 2012. Scientific Investigations Map. 2018;3406:1-16. https://doi.org/10.3133/sim3406.
35. Srivastava PK, Bhattacharya BK, Patel P, Kundu N, Sahoo RN. Evaluating the performance of back-propagation learning algorithm of an artificial neural network for the retrieval of leaf area index from IRS-P6 LISS-IV data. International Journal of Applied Earth Observation and Geoinformation. 2012;18:47-57. https://doi.org/10.1016/j.jag.2012.01.004.
36. Storie CD, Bullock EL, Brissette MB, Sesnie SE. Integrating Google Earth Engine and R for flexible, reproducible, and scalable vegetation mapping. Ecological Informatics. 2020;55:101017. https://doi.org/10.1016/j.ecoinf.2019.101017.
37. Strong ML, Fulton DC, Lupi F, Poudyal NC, Beier CM, Jordan K. Modeling public support for wildlife habitat conservation in the Great Lakes Region. PLOS ONE. 2018, 13(1). https://doi.org/10.1371/journal.pone.0191400.
38. Tan H, Wang X, Liang S. A new method to identify leaf and canopy clumping index from hyper-temporal multi-angle remote sensing data: A case study of MODIS BRDF product over the Heihe River Basin. Remote Sensing. 2016;8(3):180. https://doi.org/10.3390/rs8030180.
39. Tian Q, Yue T, Zhu L, Clinton N, Imhoff M. Urbanization dynamics in the southeastern U.S. from 1992 to 2015 using Landsat time-series data. Remote Sensing. 2019;11(5):544. https://doi.org/10.3390/rs11050544.
40. Wang P, Wang C, Liu Z, Zhou J, Chen S. Detecting urban forest phenology in a high-density urban center using Sentinel-2A imagery and Google Earth Engine. Remote Sensing. 2020;12(8):1320. https://doi.org/10.3390/rs12081320.
41. Wolniewicz M. Application of NDVI and Sentinel-2 satellite data to determination of changes in vegetation cover in the Upper Silesian Industrial Region (Poland). Journal of Ecological Engineering. 2018;19(2):186-193. https://doi.org/10.12911/22998993/83565.
42. Wu W, Wang S, Wu C, Wang J, Tan J, Zhai D, *et al*. A simple NDVI-based approach to predict daily rice evapotranspiration over large areas and its application to yield estimation. Agricultural Water Management. 2017;188:140-152. https://doi.org/10.1016/j.agwat.2017.04.003.
43. Zhang Y, Liu X, Cao L, Hong Y, Nan Z. Comparison of Four Machine Learning Algorithms for Spatial Downscaling of SMAP Soil Moisture Using Google Earth Engine. Water. 2019;11(1):210. https://doi.org/10.3390/w11010210.